Management zone delineation replacing yield maps with vegetation indices: effects of spatial resolution and machine learning-based selection

M. S. Gelain[1]; L. G. G. Sterle[1]; J. P. Molin[1]

[1]Laboratory of Precision Agriculture, "Luiz de Queiroz" College of Agriculture – University of São Paulo, SP, Brazil

A paper from the Proceedings of the
17th International Conference on Precision Agriculture and
11th Brazilian Congress on Precision and Digital Agriculture
13-16 July 2026
Porto Alegre, Brazil

Abstract.
The delineation of Management Zones (MZs) is a precision agriculture strategy that exploits the spatial variability of crop fields to support more efficient and sustainable site-specific management practices. Traditionally, yield maps have been used as one of the main information layers in this process, as they integrate the effects of soil, climate, and management throughout the crop cycle. However, obtaining reliable yield maps still presents limitations, such as the need for onboard sensors, frequent calibration, data filtering, and dependence on consistent historical yield records. In parallel, advances in remote sensing have enabled the acquisition of vegetation indices (VIs) at different spatial resolutions, with higher temporal frequency and lower operational costs. Nevertheless, the direct or isolated replacement of yield layers by VIs in MZ delineation still requires validation, particularly regarding their ability to generate zones with spatial coherence, stability, and agronomic quality comparable to those obtained from yield maps. Therefore, this study evaluated the effects of using VIs as proxy or complementary layers to yield, as well as the influence of spatial resolution, on MZ delineation. The study was conducted in nine center-pivot irrigated fields in São Paulo State, Brazil, totaling 450 ha, where management zones are known to differ from those in rainfed systems. The analysis comprised two scenarios: (i) the first growing season with soybean and (ii) the second growing season with sorghum and wheat. Images were acquired from the Sentinel Hub and PlanetScope platforms for the calculation of 14 VIs. In addition, elevation, cation exchange capacity, hydrogen potential, and organic matter data were used. MZs were generated under two treatments: the first using the most recent yield layers, and the second using four selected VIs. The selection of the most representative VIs, considering the acquisition period with the highest correlation with yield, was performed using the XGBoost machine learning model. Zone delineation was carried out using the unsupervised machine learning algorithm fuzzy c-means, and evaluated using qualitative metrics of classification entropy, degree of separation, and variance reduction, in addition to structural similarity analysis between treatments. The results indicated a high correlation ($R^2 > 0.81$) between VIs and yield, due to the large sample size at the pixel level, with CRI1 and IRECI standing out among the indices in the crop averages. Clustering resulted in MZs with distinct degrees of separation and sharpness; however, moderate structural similarity was observed in scenario (ii). In contrast, similarity was low in scenario (i), highlighting that VI-based MZs do not always reproduce yield-based spatial patterns. Scenario (ii) also presented greater saturation of the analyzed indices, which may limit the model's ability to describe crop behavior over time. The assessment of spatial resolution, focused on two fields, showed that higher spatial detail may intensify edge and

boundary effects, although it also increased average similarity between treatments. Therefore, future studies are required to evaluate edge effects as well as the influence of irrigation on VIs, and the use of VIs for MZ delineation is recommended in a moderate and/or complementary manner.

Keywords.
Fuzzy C-Means, Remote sensing, Irrigated Crop, XGBoost and Soybean.

1. Introduction

Exploring the spatial variability present within a crop field enables decision-making to be carried out in a site-specific manner within the production area, a concept that constitutes one of the fundamental bases of precision agriculture (PA) (Khosla et al. 2008; Molin et al. 2015). By identifying different productive characteristics across the area, it becomes possible to define localized management strategies adapted to the specific conditions of each region within the field (Kerry et al. 2024; Silva et al. 2025). The adoption of differentiated field management strategies has the potential to improve resource-use efficiency, profitability, and the sustainability of agricultural systems through the integration of data collection, analysis, and decision-making (Colaço et al. 2020). However, although sensing technologies have expanded the capacity to diagnose spatiotemporal variability, challenges remain in converting maps and databases into practical decisions applicable to agricultural management (Mulla 2013; Pathak et al. 2019).

The combination of data enables the development of strategies for localized crop management, such as cell-based management, differentiated management zones (MZs), and even detailed pixel-based management (Miao et al. 2018; Molin et al. 2015). Among these approaches, the use of MZs stands out because it allows the delimitation of regions with lower internal variability and greater temporal stability, capable of representing the response potential of the area across different production years (Massruhá et al. 2020; Nawar et al. 2017). Thus, MZs simplify management by grouping applications, treatments, and interventions into regions of greater similarity, while exploiting spatial variability in a more operational and precise manner (Kerry et al. 2024; Ouazaa et al. 2022).

For the delimitation of MZs, it is essential to understand the phenomena occurring within the area by identifying the intrinsic potential of the soil and its interaction with the crop (Farid et al. 2016; Li et al. 2025). In this process, layers representing relevant attributes are used, such as soil texture, apparent electrical conductivity, soil fertility, and the yield history of one or more crops (Nawar et al. 2017). However, obtaining high-quality yield maps depends on calibrated sensors, consistent data series, and rigorous preprocessing steps, such as the filtering of erroneous data (Maldaner et al. 2021; Molin et al. 2015). These requirements represent a challenge for producers, especially due to the recurrent calibration needed for sensors installed on harvesters to ensure data accuracy (McNaull and Darr 2020). Therefore, there is a growing demand for alternative or complementary methods that allow productive variability to be explored in a practical, reliable, and accessible way (Anderegg et al. 2024; Pathak et al. 2019).

In this context, remote sensing has gained increasing relevance because it enables the characterization of soil spatial variability and crop vegetative vigor, contributing to the design of localized management strategies (Breunig et al. 2020; Georgi et al. 2017; Weiss et al. 2020). The spectral response of crops is associated with the absorption and reflectance of radiation by pigments such as carotenoids, xanthophylls, and chlorophylls, allowing inferences about crop vegetative status through vegetation indices (VIs) (Mohammed et al. 2019). These indices, derived from operations between different bands of the optical spectrum, may be related to canopy development, biomass accumulation, and crop productive performance (Badgley et al. 2017; Maimaitijiang et al. 2019). However, their representativeness may vary according to species, canopy architecture, and phenological stage, making it necessary to evaluate their ability to serve as proxies for, or complements to, yield maps in the generation of MZs (Amaral et al. 2024; Cunha et al. 2024).

Therefore, this study aimed to evaluate the potential of VIs as partial substitutes or complements to yield maps in the generation of MZs. Specifically, it sought to select the VIs and acquisition periods most closely related to yield, compare the MZs obtained from yield history with those derived from VIs, and evaluate their structural quality, spatial similarity, and the influence of spatial resolution on segmentation. In doing so, this study aims to define the potential of VIs applied to PA-based management, contributing to making MZ generation more accessible and practical for farmers.

2. Materials and Methods

2.1. Study Area

This study was conducted in areas made available to the Precision Agriculture Laboratory, ESALQ-USP. Nine fields were evaluated, totaling 450 ha. All fields were irrigated by center pivot and located in the municipalities of Itaí and Itapeva, in the state of São Paulo, Brazil (Figure 1), with mean altitudes ranging from 654 to 684 m. According to the Köppen classification, the local climate is Cwa, characterized as humid subtropical with a dry winter (Alvares et al. 2013). Mean annual precipitation ranges from 1,252 to 1,377 mm, and mean temperature ranges from 20.4 to 20.7 °C for Itapeva and Itaí, respectively. The soil is predominantly classified as a dystrophic Red Latosol with clayey texture. These areas are managed under a crop rotation system, with soybean, sorghum, wheat, and barley as the predominant crops.

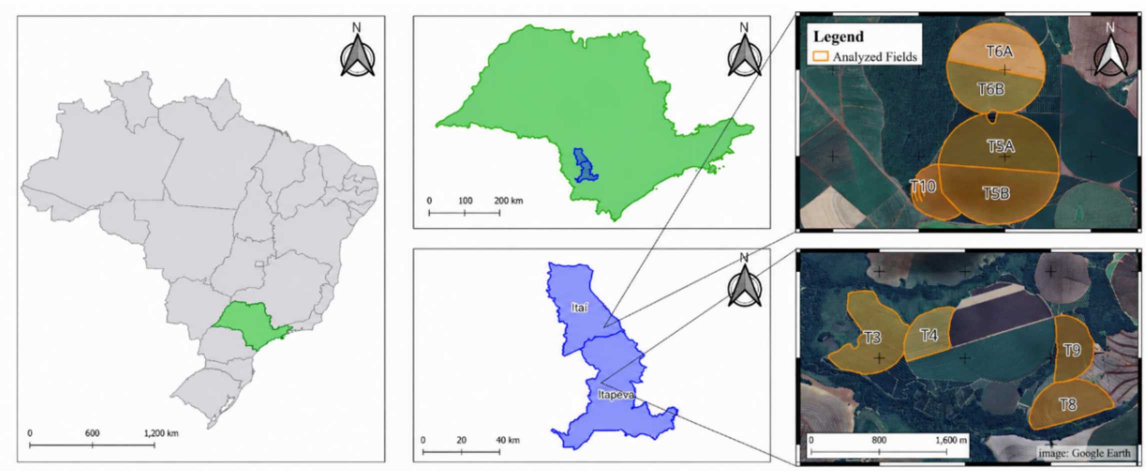

Fig. 1 Analyzed areas, in which T5A and T5B have 80 ha; T6A has 55 ha; T6B has 53 ha; T10 has 23 ha; T4 has 28 ha; T3 has 59 ha; T8 has 41 ha; and T9 has 31 ha.

2.2. Soil and Yield Data Acquisition

Soil sampling was performed at a depth of 0–0.20 m using a sampling grid of approximately one point every 2 ha. Each composite sample consisted of five subsamples collected within a 5-m radius. The composite samples were then sent to the laboratory for chemical analysis. Samples from fields 5A, 6A, 8, and 9 were collected in February 2024; those from fields 5B and 10 in April 2023; field 3 in January 2022; field 4 in December 2021; and field 6B in March 2017. The soil attributes analyzed were organic matter (OM), hydrogen potential (pH), phosphorus (P), potassium (K), calcium (Ca), magnesium (Mg), cation exchange capacity (CEC), base saturation (V%), and sulfur (S). Elevation data were extracted from the digital elevation model (DEM) generated from elevation points collected by the GNSS receiver installed on the harvester.

The available yield layers were obtained from a harvester equipped with a yield monitor. Data from the 2019, 2021, 2022, 2023, 2024, and 2025 growing seasons were evaluated. For all seasons, filtering was performed using MapFilter 2.0 software (Maldaner et al. 2021), removing erroneous data and outliers. For statistical filtering, the maximum median variation parameter was set at 50%, while for local filtering it was set at 75%, with a spatial dependence of 89.5 m, corresponding to ten times the width of the harvester platform. Finally, yield points were interpolated by kriging using the SmartMap plugin in QGIS.

2.3. Remote Sensing Dataset

Remote sensing data were obtained from the Sentinel-2 L2A platform, MSI sensor with 10 m spatial resolution, and PlanetScope, SuperDove sensor with 3 m spatial resolution. For this purpose, the best images were selected, with a maximum cloud cover of 30%. The search was conducted between sowing and harvest, with all images having atmospheric correction. Only images that met the maximum cloud-cover threshold for the requested period were selected. After each image request, the 14 desired indices (Table 1) were calculated and saved using a Python script, together with the bands used and RGB images for later verification.

Table 1 Vegetation indices evaluated.

Acronym	Name	Formula
CI	Chlorophyll Index	(RE / R) - 1
CRI1	Carotenoid Reflectance Index	(1 / RE) - (1 / RE2)
EVI	Enhanced Vegetation Index	2.5 * (NIR - R) / (NIR + 6 * R - 7.5 * B + 1)
EVI2	Enhanced Vegetation Index 2	2.5 * (NIR - R) / (NIR + R + 1)
GNDVI	Green Normalized Difference Vegetation Index	(NIR - G) / (NIR + G)
GVI	Green Vegetation Index	((2G) – R - B) / ((2R) +G +B)
IRECI	Inverted Red-Edge Chlorophyll Index	(RE2 - R) / (RE1 / RE2)
MTCI	MERIS Terrestrial Chlorophyll Index	(RE1 – RE2) / (RE1 - R)
NDMI	Normalized Difference Moisture Index	(NIR - SWIR) / (NIR + SWIR)
NDRE	Normalized Difference Red Edge Index	(NIR - RE) / (NIR + RE)
NDVI	Normalized Difference Vegetation Index	(NIR - R) / (NIR +R)
PSRI	Plant Senescence Reflectance Index	(R - B) / RE
PSSR	Pigment-Specific Simple Ratio	NIR / R
SAVI	Soil-Adjusted Vegetation Index	((NIR - R) / (NIR + R + L)) * (1 + L)
SFDVI	Spectral Feature Depth Vegetation Index	((NIR + G) / 2 - (R + RE) / 2)

** Where: B = blue band; G = green band; NIR = near-infrared band; R = red band; RE = red-edge band; RE1 = band centered at 708.4 nm; RE2 = band centered at 747.6 nm.*

PlanetScope images were acquired manually, selecting only those without cloud cover over the analyzed fields. Due to the limited number of available scenes, suitable images were obtained for fields 6A and 6B for the 2025, 2024, 2023, 2022, and 2021 growing seasons. After image selection, the vegetation indices were calculated. However, the PlanetScope platform does not provide all spectral bands available in Sentinel-2. For this reason, indices such as NDMI and CRI1 could not be calculated, while IRECI and MTCI had to be adapted as follows:

$$IRECI = \frac{Nir - Red}{Rededge} \tag{1}$$

$$MTCI = \frac{Nir - Red}{Red - Rededge} \tag{2}$$

To define the period of greatest representativeness of yield, the vegetation indices were grouped into acquisition windows corresponding to 20-day intervals after sowing, allowing comparison among growing seasons and platforms with different imaging dates. Each index was evaluated individually using XGBoost models, with the aim of identifying the acquisition periods with the greatest ability to represent the spatial variability of yield.

For the models based on Sentinel data, 257,958 sample points extracted from raster pixels were used. Model evaluation was performed using hold-out validation, with a random split of 70% of the data for training and 30% for validation. Performance was measured using R^2, RMSE, and MAE. It should be noted that, because data from the same area and growing season were used for training and testing, this approach mainly evaluates the retrospective spatial interpolation capacity of the models (Filippi et al. 2024).

The temporal groups with the best predictive performance were considered the ideal image acquisition periods, that is, those in which the vegetation indices best represented the spatial variability of yield. Based on this selection, a new XGBoost model was developed by integrating the indices belonging to the selected groups, allowing identification of the four most relevant vegetation indices for describing the spatial pattern of yield.

2.4. Delimitation and Evaluation of MZs

The delimitation of MZs was performed using the Fuzzy C-Means (FCM) algorithm (Sterle and Molin 2025), with the fuzzy exponent set to 1.25, a maximum of 100 iterations, and a smoothing degree of 3 as default parameters. The optimal number of clusters was defined based on the NCE (Moharana et al. 2020), and VR (Sterle and Molin 2025) indices, considering the greatest increase in variance reduction as the main criterion and, in cases of proximity between solutions, the lowest FPI and NCE values.

The quality of the MZs was evaluated in terms of internal homogeneity, separability among classes, and structural similarity among maps. For this purpose, the FPC (Fuzzy Partition Coefficient), NCE (Normalized Classification Entropy), and VR (Variance Reduction) indices were used, in addition to ARI and NMI indicators, which were employed to compare the spatial and structural agreement among MZs generated from different datasets. ARI was used as a more rigorous point-to-point agreement metric, whereas NMI was used to assess the overall similarity among partitions (Shilpa et al. 2025). The interpretation of these indices was based on performance classes ranging from random segmentation to complete similarity (Table 2). To identify the relative contribution of the variables used in MZ formation, a Random Forest model was fitted using the layers included in each scenario, allowing the importance of each attribute in cluster delimitation to be estimated.

Table 2. ARI and NMI classes used to evaluate structural performance among MZs generated under different treatments.

Range	Performance
1.0 to 0.8	Complete similarity
0.8 to 0.6	High similarity
0.6 to 0.4	Moderate similarity
0.4 to 0.2	Low similarity
0.2 to 0.0	Random segmentation

2.5. Analysis of Yield Replacement by VIs

The influence of replacing the yield layer with vegetation indices was evaluated by comparing two datasets: one based on yield maps and another composed of the four most relevant vegetation indices previously selected by the predictive models. In both cases, complementary layers of elevation, organic matter, and CEC were added. This analysis was performed individually for each field and repeated under two production scenarios, corresponding to the summer season and the winter season. For each scenario, NCE, and VR were calculated. These indices were subjected to normality and homogeneity tests and subsequently compared using Student's t-test at 5% significance.

The influence of spatial resolution on MZ quality was evaluated by comparing the clusters generated from the best vegetation indices obtained from Sentinel, with 10 m resolution, and PlanetScope, with 3 m resolution. This step was conducted in fields 6A and 6B, using historical growing-season series from 2021 to 2025. As an additional reference, MZs were also generated using only yield layers at 10 m and 3 m resolutions. For all clusters, NCE, and VR were calculated. After checking normality, the results were subjected to Tukey's mean comparison test at 5% significance, allowing the effect of spatial resolution on cluster quality and coherence to be evaluated.

3. Results and Discussion

3.1. Influence of Replacing Yield by VIs

Table 3 presents the predictive performance of the different VIs in estimating the yield of soybean, sorghum, and wheat crops, obtained through spatial interpolation using XGBoost models. The indices showed high explanatory capacity for the three crops, with R^2 values ranging from 0.81 to 0.93, indicating a strong relationship between the spectral indices and the observed yield. This high performance resulted from the large volume of autocorrelated data, in which model performance may be inflated when training and validation data come from the same spatial and temporal context (Filippi et al. 2024). For soybean, the best performances were obtained by the IRECI, SAVI, SFDVI, and EVI2 indices (R^2 = 0.91), which also showed the lowest prediction errors, with mean RMSE of 0.441 and MAE of 0.327. In contrast, the lowest performances were observed for MTCI, CI, GNDVI, and GVI. It is important to highlight that GVI is constructed exclusively from bands in the visible spectrum, which are inherently less sensitive to physiological and structural crop variability than red-edge and near-infrared bands, which are more responsive to changes in biomass, chlorophyll content, and leaf structure (Lin et al. 2019). Therefore, indices based only on the visible spectrum tend to provide lower discriminatory capacity, since the red-edge and near-infrared regions may be more closely correlated with leaf structure, particularly the mesophyll, and photosynthetic activity.

Table 3. Performance of each vegetation index in modeling the spatial variability of crop yield, evaluated by hold-out validation in machine learning models.

Index	Soybean			Wheat			Sorghum		
	R^2	RMSE	MAE	R^2	RMSE	MAE	R^2	RMSE	MAE
CI	0.89	0.48	0.35	0.92	0.35	0.24	0.81	1.24	0.92
CRI1	0.9	0.46	0.33	0.92	0.35	0.24	0.9	0.92	0.67
EVI	0.9	0.45	0.34	0.92	0.35	0.24	0.88	1.00	0.73
EVI2	0.91	0.45	0.33	0.88	0.42	0.29	0.88	0.97	0.71
GNDVI	0.89	0.48	0.34	0.9	0.39	0.27	0.86	1.08	0.78
GVI	0.89	0.48	0.36	0.92	0.35	0.24	0.83	1.19	0.87
IRECI	0.91	0.43	0.32	0.92	0.35	0.24	0.89	0.94	0.68
MTCI	0.89	0.49	0.36	0.92	0.34	0.23	0.84	1.15	0.85
NDMI	0.9	0.46	0.34	0.89	0.41	0.28	0.88	0.98	0.71
NDRE	0.9	0.47	0.34	0.89	0.4	0.28	0.87	1.02	0.73
NDVI	0.9	0.46	0.34	0.91	0.36	0.26	0.87	1.03	0.74
PSRI	0.89	0.48	0.36	0.92	0.34	0.23	0.83	1.16	0.87
PSSR	0.9	0.46	0.34	0.92	0.35	0.24	0.87	1.03	0.74
SAVI	0.91	0.44	0.33	0.92	0.34	0.24	0.88	0.98	0.71
SFDVI	0.91	0.45	0.33	0.92	0.36	0.24	0.88	0.97	0.70

For the winter crops, a distinct pattern was observed in relation to the vegetation indices. In sorghum, although some indices showed high overall performance, with R^2 values ranging from 0.81 to 0.90, the RMSE and MAE values were higher. Considering the mean yield of 9.91 t ha^{-1}, model errors represented from 12.53%, for the highest RMSE of 1.24, to 9.23%, for the lowest RMSE of 0.92. In contrast, wheat showed the highest R^2 values, with emphasis on CRI1, SAVI, EVI, and NDRE, all with R^2 values above 0.92. The mean error was notably low, representing 4.86% of the crop mean yield of 6.78 t ha^{-1} when RMSE was 0.33, and 6.34% when RMSE was 0.42. The lower performance of the XGBoost model in predicting sorghum yield may be associated with the methodological approach adopted. Because the modeling was performed using yield observations from both winter crops simultaneously, the model had to handle two different yield magnitudes, canopy structures, and spectral dynamics. This heterogeneity may introduce additional unexplained variation and hinder the learning process of crop-specific patterns. As a result, the algorithm's ability to establish consistent relationships between vegetation indices and actual sorghum yield may have been reduced.

In addition, crops with contrasting architectures, such as wheat, which has a more uniform canopy and intermediate biomass, and sorghum, which is characterized by taller plants and greater sensitivity to lodging, tend to respond differently to the same spectral indices. According to Verrelst et al. (2019), machine learning models tend to perform better when trained specifically for each crop. This represents a preventive measure to avoid increasing noise in the model, since combining different crops may generate a mixture of physiological patterns. Thus, when yield information from different crops is combined in a single model, part of the species-specific variability may be omitted. However, grasses generally show greater prediction potential than legumes because their biomass more directly reflects yield potential, a characteristic that is not always observed in crops such as soybean (Canata et al. 2021; Fiorio et al. 2024). Therefore, prediction models based on vegetation indices often show better results for grasses. For example, Ahmadi et al. (2025) reported high performance in wheat yield prediction using Random Forest models with indices such as NDVI, SAVI, and EVI, obtaining R^2 values between 0.91 and 0.96 and low RMSE values ranging from 0.10 to 0.16 Mg ha^{-1}, like those observed in the present study. In contrast, for soybean, Yu et al. (2025) reported R^2 values ranging from 0.60 to 0.91 when using Random Forest to predict yield based on variability in visible bands, but with high RMSE values ranging from 0.54 to 1.04 Mg ha^{-1}.

It is worth noting that center-pivot irrigation management may have partially attenuated the discriminatory capacity of water-sensitive indices, particularly NDMI. Under irrigation system, soil water availability tends to be spatially homogenized throughout the field, reducing the natural gradients that moisture-based indices are designed to detect. As a result, the spectral response of canopy structure and chlorophyll content, captured via red-edge and NIR based indices, become more relevant drivers of spectral yield relationships than water content signals under irrigated conditions. This behavior may explain why structurally and pigment sensitive indices, like IRECI, SAVI, and EVI2, consistently outperformed moisture related indices in soybean yield prediction across the evaluated fields. Furthermore, saturation effects in high biomass irrigated crops, such as sorghum and wheat, may reduce the sensitivity of traditional VIs to subtle spatial variability. Therefore, future studies should compare VI performance under irrigated and rainfed conditions to better isolate the role of water availability in spectral responses and management zone delineation.

Figure 2 presents the temporal behavior of the vegetation indices and their respective SHAP importance values across image acquisition groups for soybean. Overall, the groups between 80 and 120 days after sowing, corresponding to groups 5 and 6, contributed the most to yield estimation. This period generally coincides with the grain-filling stages, between R5 and R6, when the crop directs a large proportion of photoassimilates to grain formation and, therefore, tends to show a stronger relationship with final yield (Kross et al. 2020). However, the vegetative peak of the indices occurred before the groups with the greatest importance for the model. This result indicates that the highest mean VIs value does not necessarily represent the best timing for image acquisition aimed at yield estimation. Thus, defining the optimal imaging window should consider not only maximum vegetative vigor but mainly the phenological stage in which spectral variation is most strongly associated with yield components and final yield variability within the field. For sorghum and wheat, the most relevant acquisition groups occurred, on average, between 80 and 100 days after sowing, a period associated with the end of flowering and grain filling. However, unlike soybeans, rapid canopy closure and high biomass favored the saturation of some indices, reducing their sensitivity to discriminate against small spatial variations at more advanced stages of the crop cycle (Huete et al. 1997). In wheat, despite high R^2 values, the formation of a temporal plateau indicates low variation in VIs over the analyzed period. This may increase redundancy among indices with similar behavior, such as NDVI, EVI, and MTCI, and increase the risk of model overfitting. Nevertheless, the SHAP analysis demonstrated that indices with similar mean curves may contribute differently due to the different spatial distributions captured by each index. Therefore, combining VIs sensitive to different canopy properties, such as biomass, pigments, vegetation structure, and plant moisture, proved important for better representing the spatial variability of crops and increasing the robustness of yield estimates.

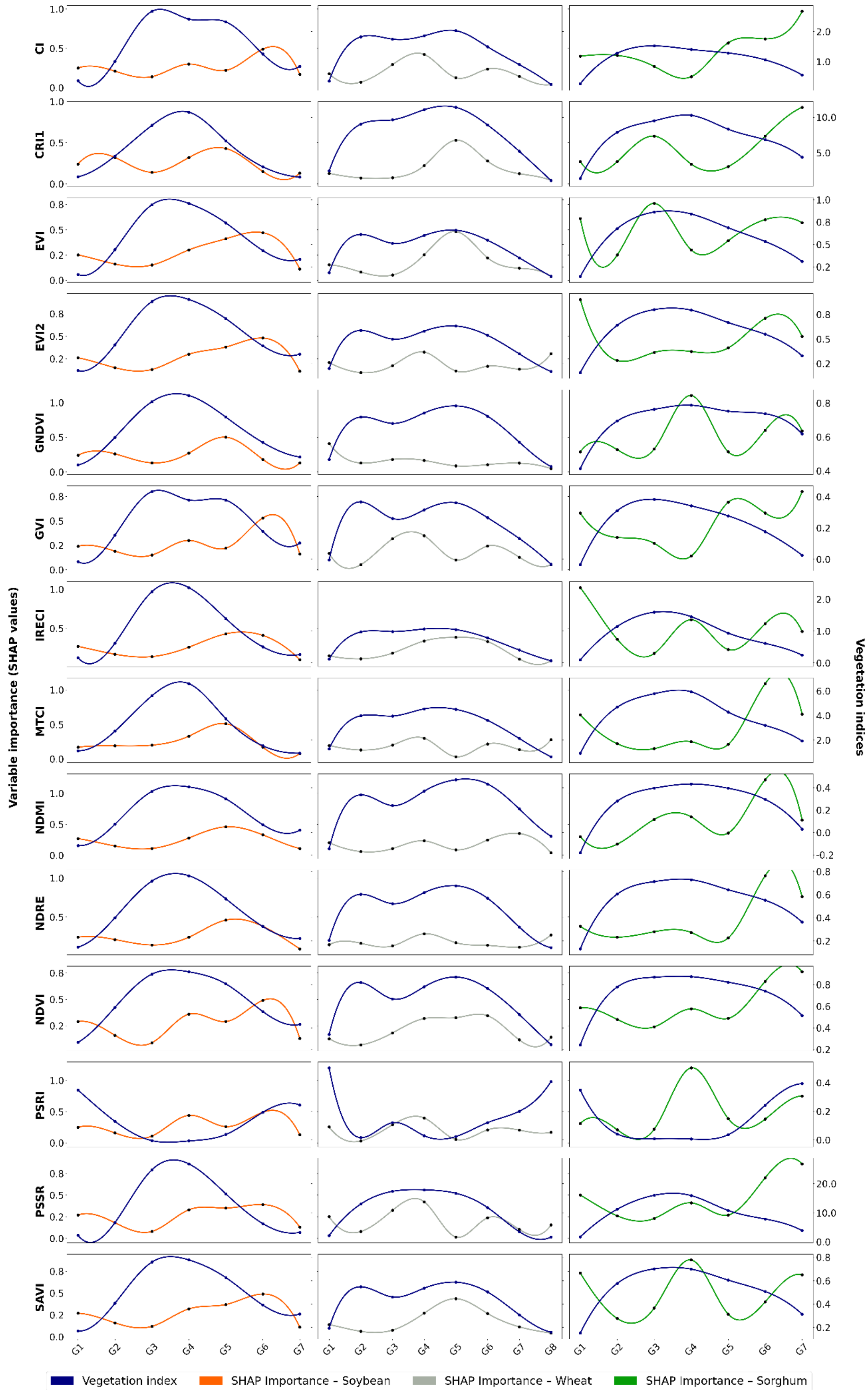

CI
CRI1
EVI
EVI2
GNDVI
GVI
IRECI
MTCI
NDMI
NDRE
NDVI
PSRI
PSSR
SAVI
Variable importance (SHAP values)
Vegetation indices
Vegetation index
SHAP Importance - Soybean
SHAP Importance - Wheat
SHAP Importance - Sorghum

Fig. 2 Representation of the behavior of vegetation indices and SHAP importance values across image acquisition groups, from group 1 to group 7, for soybean, sorghum, and wheat.

Figure 3 presents the importance of the variables selected for the final soybean yield prediction model, evaluated using the SHAP algorithm. The selection of indices aimed to combine complementary information related to moisture, pigments, and vegetative vigor, thereby reducing limitations associated with the saturation of traditional indices. Among the variables evaluated, NDMI obtained between 80 and 100 days after sowing stood out as the main predictor. However, its isolated use should be interpreted with caution, as vegetation indices may present limitations at stages of high canopy closure and high biomass, when spectral sensitivity to discriminate small spatial variations is reduced (Huete et al. 1997). The final model showed good predictive performance, with R^2 of 0.87, RMSE of 0.53, and MAE of 0.38. This result was supported by the integration of multiple fields during training, which expanded the variability represented by the model, favored the identification of more general patterns, and reduced the risk of overfitting.

In addition, indices commonly reported in the literature, such as SAVI, EVI, and NDVI, showed lower contribution for soybean, whereas pigment-related indices, such as CRI1, IRECI, and PSRI, presented greater importance. This behavior suggests that, due to the physiological plasticity of soybean, variations related to pigment dynamics may better represent the spatial variability of the crop than purely vegetative indices. For winter crops, the pattern was different. In sorghum and wheat, vegetative indices such as GNDVI, SAVI, CI, and NDVI showed greater importance, reflecting the more direct relationship between biomass and yield in these crops. This behavior is consistent with the more uniform architecture and higher plant population density of grasses, in which yield variation tends to be better captured by indices related to canopy vigor and biomass (Canata et al. 2021).

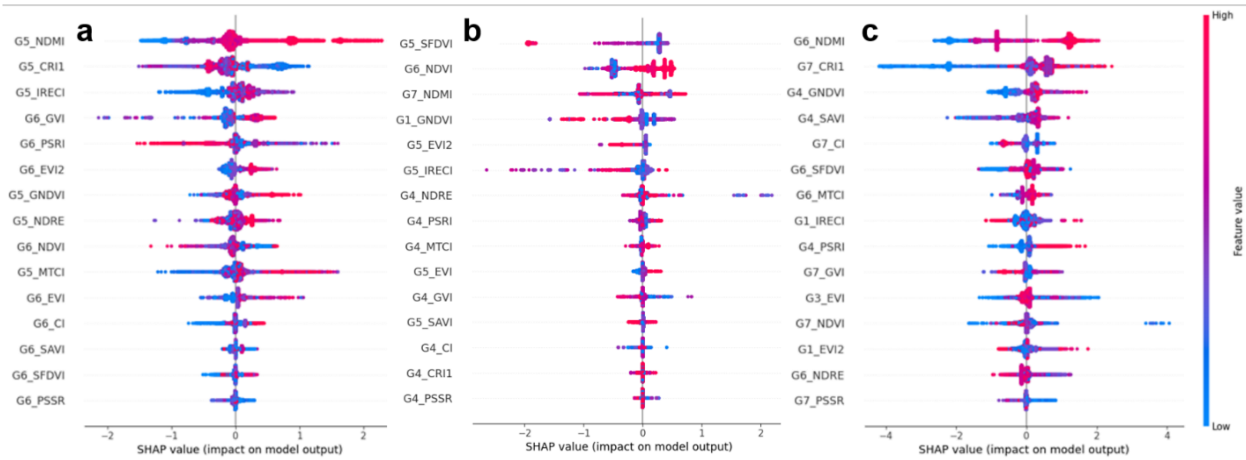

Fig. 3 Importance of the variables in explaining soybean (a), wheat (b), and sorghum (c) yield according to the machine learning model evaluated using the SHAP algorithm.

Table 4 presents the validation indices of the quality of MZs constructed from VIs and yield layers, considering four clusters. In the summer season, no statistical differences were observed between treatments for the evaluated indices, indicating that VIs were able to generate MZs with quality similar to those obtained from yield data. This behavior demonstrates that the selected indices represented part of the spatial variability within the fields, even considering the limitations associated with VI saturation in crops with higher biomass. In the winter season, NCE and VR remained statistically similar between treatments, whereas FPC showed differences. Nevertheless, the values obtained remained close, indicating that the segmentations generated from VIs maintained internal coherence in relation to the zones constructed from yield data. Therefore, the selected VIs showed potential as complementary or proxy layers for MZ generation. However, this use should be interpreted with caution, since spectral behavior may vary according to crop type, field conditions, and the presence of different physiological and structural canopy patterns (Amaral et al. 2024; Rokhafrouz et al. 2021).

Table 4. Mean validation indices of the quality of MZs obtained from vegetation index layers and MZs generated from yield

layers, with the optimal number of clusters set to four, under two scenarios. Different letters within the same scenario differ by Student's t-test at 5% significance.

Index	Summer season		Winter season	
	VI	Yield	VI	Yield
NCE	0.13 a	0.16 a	0.17 a	0.13 a
FPC	0.90 a	0.88 a	0.87 a	0.90 b
VR	0.67 a	0.58 a	0.54 a	0.70 a

From Figure 4, it is possible to observe the influence of replacing yield layers with layers derived from vegetation indices. For some fields, such as 3, 4, and 6B, the VIs expressed a spatial behavior similar to that of the yield layers. In these cases, common attributes among treatments, such as soil fertility and elevation, had greater weight in zone delimitation. In contrast, more pronounced differences among treatments were observed in the remaining fields, indicating that MZs generated exclusively from VIs tend to emphasize edge regions. This pattern reflects a limitation in the use of images as direct substitutes for yield layers, since field edges present abrupt changes in vegetative behavior. This phenomenon was observed in field 9, where internal variability was masked by the strong vegetative contrast present along the edge. This condition may be related to the limited spatial resolution of the images, in which each pixel represents approximately 100 m², favoring spectral mixing between native vegetation, unmaintained roads, and cultivated vegetation. This mixture impairs the real representation of the field, compromising the accuracy of MZs generated from VIs.

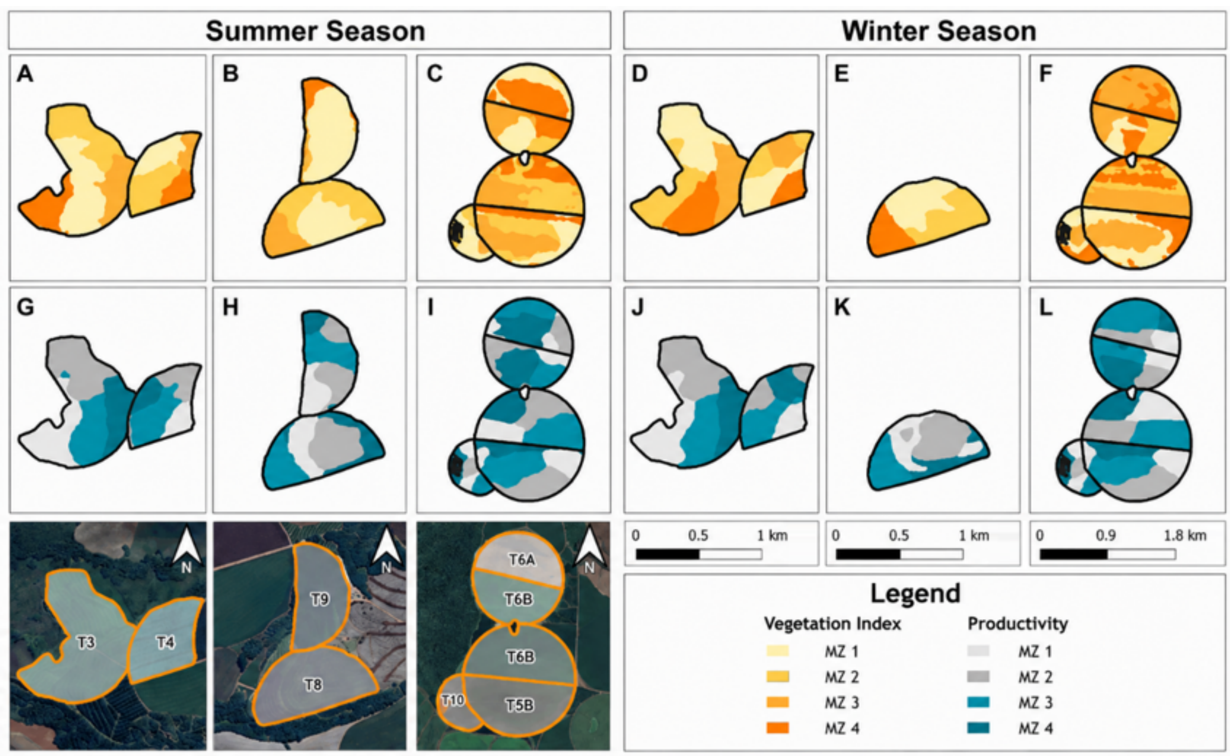

Fig. 4 Representation of fields 3, 4, 5A, 5B, 6A, 6B, 8, 9, and 10 segmented into four clusters. Panels A, B, and C represent zoning performed using soybean vegetation index data; panels D, E, and F represent zoning performed using sorghum and wheat vegetation index data. Panels G, H, and I represent zoning performed using soybean yield data, whereas panels J, K, and L represent zoning performed using sorghum and wheat yield data.

Table 5 shows the similarity indices between the MZs generated from VIs and those obtained from yield data under the summer and winter season scenarios. Overall, the ARI and NMI values indicate low to moderate similarity between the methods, with an average increase from the summer season to the winter season. ARI increased from 0.33 to 0.44, while NMI increased from 0.38 to 0.47, suggesting that the VIs showed greater spatial correspondence with yield in the second evaluated period. Despite this general pattern, similarity varied among fields. Fields 3, 4, and 6B showed greater agreement between the MZs, with field 4 standing out in the winter season, reaching ARI and NMI values of 0.83. This result indicates strong correspondence between the spatial patterns generated by the two methods, possibly associated with the greater influence of common layers, such as soil fertility and elevation, and lower interference from edge effects.

Table 5. Similarity indices between MZs obtained from vegetation index layers and MZs generated from yield layers under two scenarios. ARI: Adjusted Rand Index; NMI: Normalized Mutual Information.

Field	Summer season		Winter season	
	ARI	NMI	ARI	NMI
3	0.5	0.59	0.76	0.75
4	0.59	0.6	0.83	0.83
5A	0.34	0.33	0.32	0.38
5B	0.2	0.25	0.3	0.29
6A	0.29	0.24	0.27	0.21
6B	0.51	0.6	0.36	0.46
8	0.31	0.4	0.34	0.44
9	0.14	0.23	-	-
10	0.06	0.16	0.33	0.41
Mean	**0.33**	**0.38**	**0.44**	**0.47**

In contrast, fields such as 5B, 6A, 9, and 10 showed lower similarity, indicating that the VIs generated zones with spatial distributions different from those obtained from yield data. This behavior may be related to the greater sensitivity of VIs to edge effects and to the weaker direct correspondence between vegetative vigor and yield, especially in crops with greater physiological plasticity. In addition, irrigation effects may add a layer of noise to the VIs. Thus, although the VIs represented part of the spatial variability within the fields, their ability to serve as direct substitutes for yield data in MZ generation proved to be dependent on the conditions of each area, the crop evaluated, and the spatial quality of the images used.

3.2. Influence of Spatial Resolution

Table 6 presents the performance of soybean yield prediction models generated using VIs derived from PlanetScope, with 3 m spatial resolution, and Sentinel-2, with 10 m spatial resolution. Overall, the models developed with PlanetScope data showed slightly higher predictive performance, with R^2 values ranging from 0.76 to 0.92 and generally lower RMSE and MAE values. This behavior indicates that higher spatial resolution increased the amount of information available for model training, mainly by increasing the number of pixels and allowing finer spatial gradients within the fields to be represented. However, this response was not uniform among indices, as observed for SFDVI, which showed lower performance with PlanetScope data. This result indicates that the advantage of higher spatial resolution depends not only on pixel size, but also on the spectral sensitivity of each index and on the acquisition period used to represent crop variability.

Table 6. Performance of each vegetation index in modeling the spatial variability of crop yield, evaluated by hold-out validation in machine learning models.

Index	PlanetScope			Sentinel		
	R^2	RMSE	MAE	R^2	RMSE	MAE
NDRE	0.9	0.29	0.22	0.89	0.32	0.24
NDVI	0.91	0.27	0.2	0.89	0.32	0.24
EVI	0.9	0.3	0.22	0.89	0.32	0.24
GVI	0.88	0.32	0.23	0.87	0.35	0.26
PSRI	0.89	0.3	0.23	0.87	0.35	0.26
SFDVI	0.76	0.45	0.36	0.89	0.31	0.23
GNDVI	0.91	0.27	0.21	0.89	0.32	0.24
SAVI	0.92	0.27	0.2	0.9	0.31	0.23
CI	0.9	0.3	0.22	0.87	0.35	0.26
MTCI	0.88	0.33	0.24	0.87	0.34	0.26
PSSR	0.91	0.27	0.2	0.87	0.34	0.25
IRECI	0.91	0.27	0.2	0.89	0.31	0.23
EVI2	0.92	0.27	0.2	0.9	0.31	0.23

After selecting the best acquisition groups, the final models showed similar explanatory capacity for both platforms, as shown in Figure 5. The model fitted with PlanetScope data presented an R^2 of 0.89 and an RMSE of 0.30, whereas the Sentinel model obtained the same R^2, but with a higher RMSE of 0.36. Thus, although both platforms were able to capture spatial patterns associated with soybean yield, the lower error observed for PlanetScope suggests greater precision in representing local variations. In both models, PSRI and MTCI showed high importance, indicating that indices related to pigment dynamics and red-edge information contributed consistently to yield prediction, regardless of the spatial resolution of the image source.

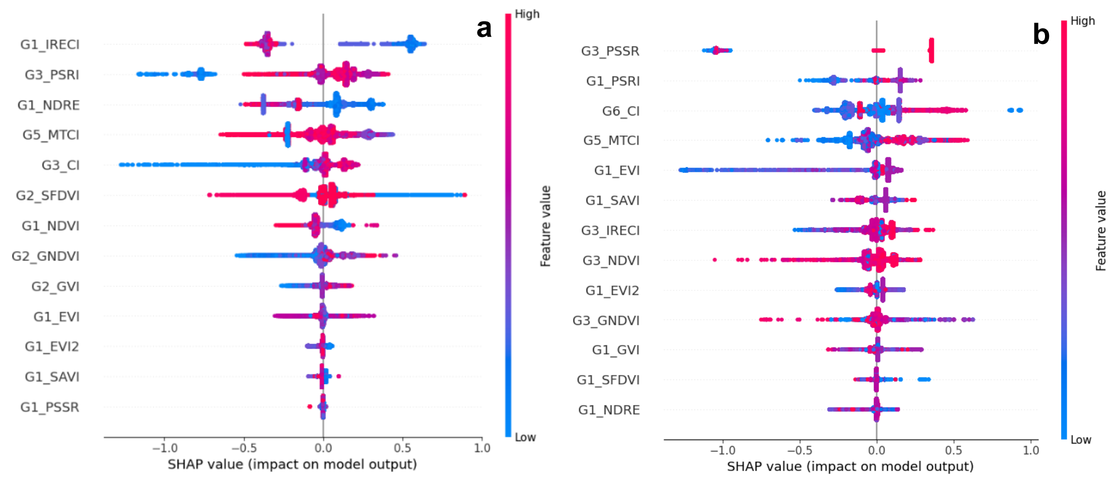

Fig. 5 Importance of the selected vegetation indices in explaining soybean yield, where (A) represents the model fitted with data obtained from the PlanetScope platform and (B) represents the model fitted with data from Sentinel, both evaluated using the SHAP algorithm.

Table 7 shows that the differences observed in predictive performance were not reflected in statistically significant differences in the fuzzy quality of the MZs. NCE, FPC, and VR did not differ among treatments, indicating that MZs generated from PlanetScope, Sentinel, and yield layers presented similar internal structure and partition quality. This result suggests that, when evaluated only by internal clustering metrics, both remote sensing platforms were able to generate zones with comparable homogeneity and separation. However, similar fuzzy quality does not necessarily imply that the spatial arrangement of the zones was equivalent among treatments.

Table 7. Mean validation indices of the quality of MZs generated from Sentinel and PlanetScope remote sensing layers, compared with MZs derived from yield layers, considering their respective spatial resolutions (Px10 = 10 m and Px3 = 3 m), in two scenarios. Different letters within the same scenario differ by Tukey's mean comparison test at 5% significance.

Index	Yield Px3		Yield Px10		PlanetScope		Sentinel	
	Field 6A	Field 6B	Field 6A	Field 6B	Field 6A	Field 6B	Field 6A	Field 6B
NCE	0.18 a	0.16 a	0.17 a	0.14 a	0.16 a	0.15 a	0.20 a	0.14 a
FPC	0.87 a	0.88 a	0.87 a	0.90 a	0.88 a	0.89 a	0.85 a	0.90 a
VR	0.59 a	0.60 a	0.41 a	0.49 a	0.47 a	0.58 a	0.47 a	0.49 a

This distinction becomes evident in Figure 6, which shows the spatial configuration of the MZs generated for fields 6A and 6B. In field 6A, the PlanetScope-based zones showed greater spatial agreement with the yield-based zones, suggesting that the 3 m resolution was more effective in capturing local variations relevant to MZ delineation. In contrast, Sentinel generated more generalized zones, probably due to the smoothing effect caused by the larger pixel size. In field 6B, however, the higher spatial detail of PlanetScope resulted in more fragmented zones, indicating that higher resolution may also increase sensitivity to small patches and local noise, requiring careful adjustment of the smoothing parameters.

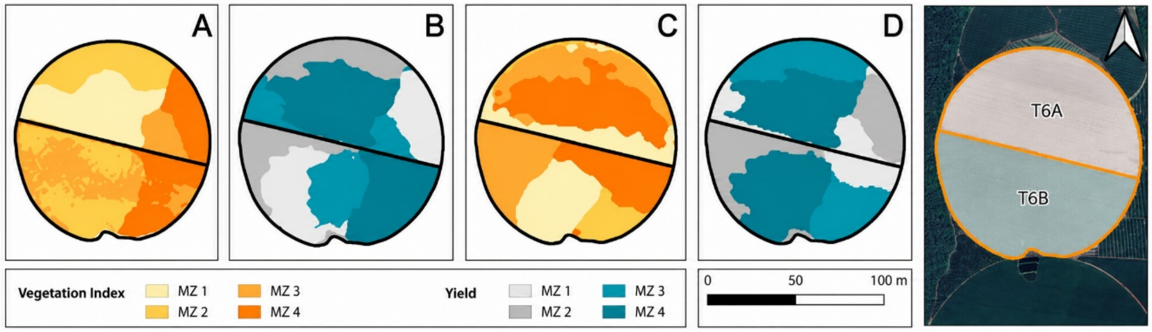

Fig. 6 Representation of fields 6A and 6B segmented into four clusters, using data from 2025 and 2024 for field 6A and from 2025 and 2023 for field 6B. (A) Zoning performed with high-spatial-resolution soybean vegetation indices (PlanetScope); (B) zoning performed with soybean yield data at 3 m pixel resolution; (C) zoning performed with soybean vegetation index data at 10 m resolution (Sentinel); and (D) zoning performed with soybean yield data at 10 m pixel resolution.

The similarity indices presented in Table 8 reinforce this interpretation. In field 6A, PlanetScope showed greater agreement with yield layers, reaching ARI of 0.67 and NMI of 0.66 when compared with yield at 10 m resolution, while Sentinel showed lower values. This indicates that, under conditions of greater internal heterogeneity, the higher-resolution imagery was more capable of reproducing the spatial structure observed in the yield maps. In field 6B, however, this pattern was less evident, and Sentinel showed better relative performance than in field 6A. This suggests that, when the spatial variability occurs in broader and more continuous patterns, medium-resolution imagery may be sufficient to represent the main structure of the field.

Table 8. Similarity indices among the MZs obtained from remote sensing images and yield layers. The MZs generated from Sentinel-2A images with 10 m spatial resolution were compared with yield layers (Px10 = 10 m), and the MZs obtained from PlanetScope images were compared with yield layers (Px3 = 3 m).

Comparison		Field 6A		Field 6B	
Layer 1	**Layer 2**	**ARI**	**NMI**	**ARI**	**NMI**
Sentinel	Yield Px10	0.26	0.23	0.46	0.52
Sentinel	Yield Px3	0.23	0.12	0.39	0.49
Sentinel	PlanetScope	0.18	0.19	0.19	0.24
PlanetScope	Yield Px10	0.67	0.66	0.24	0.3
PlanetScope	Yield Px3	0.55	0.59	0.24	0.29
Yield Px10	Yield Px3	0.77	0.77	0.53	0.67

Therefore, the influence of spatial resolution on MZ delineation was not limited to predictive performance, but was mainly related to how each platform represented the spatial structure of the field. Higher-resolution images tended to improve the detection of local variability and increase similarity with yield-based zones in more heterogeneous areas. However, they may also increase fragmentation when small-scale variations are incorporated into the clustering process. Thus, the choice between PlanetScope and Sentinel should consider not only image resolution, but also the spatial pattern of the field, the desired level of operational detail, and the need to adjust smoothing parameters during MZ generation.

4. Conclusion

This study evaluated the potential of VIs and image spatial resolution for the delimitation of MZs. The results demonstrated that, although yield remains one of the main references for zone generation, carefully selected VIs can serve as complementary or proxy layers, especially in situations where yield data are unavailable or present operational limitations. Overall, VIs derived from PlanetScope, with 3 m spatial resolution, showed a greater ability to represent the spatial variability of the fields, approaching the zones generated from yield data. Sentinel images, with 10 m resolution, proved useful for general assessments, but showed greater limitations in capturing microvariations and greater sensitivity to edge effects.

The use of VIs did not significantly compromise the internal quality of MZs in the summer season.

In the winter season, differences were observed for FPC, indicating changes in partition sharpness. Even so, the VIs were able to represent vegetative gradients related to crop performance. However, the spatial similarity between MZs generated from VIs and yield was generally low to moderate, demonstrating that this use should consider the crop, phenological stage, and type of index used. Thus, under the evaluated conditions, the use of VIs combined with soil physicochemical layers and altimetric information constitutes a promising alternative for MZ delimitation, potentially increasing the accessibility of this tool in precision agriculture. For future studies, it is suggested that MZs be generated from yield layers predicted by VIs and that the methodology be tested in rainfed areas in order to better understand the effect of irrigation on the spectral response of crops.

5. References

Ahmadi, M., Ramezani Etedali, H., Kaviani, A., & Tavakoli, A. (2025). Estimation of the yield and green water footprint of rainfed wheat based on remote sensing and machine learning. Applied Water Science 2025 15:8, 15(8), 186-. https://doi.org/10.1007/S13201-025-02542-X

Alvares, C. A., Stape, J. L., Sentelhas, P. C., De Moraes Gonçalves, J. L., & Sparovek, G. (2013). Köppen's climate classification map for Brazil. Meteorologische Zeitschrift, 22(6), 711–728. https://doi.org/10.1127/0941-2948/2013/0507

Amaral, L. R., Oldoni, H., Baptista, G. M. M., Ferreira, G. H. S., Freitas, R. G., Martins, C. L., et al. (2024). Remote sensing imagery to predict soybean yield: a case study of vegetation indices contribution. Precision Agriculture, 25(5), 2375–2393. https://doi.org/10.1007/S11119-024-10174-5/FIGURES/8

Anderegg, J., Tschurr, F., Kirchgessner, N., Treier, S., Graf, L. V., Schmucki, M., et al. (2024). Pixel to practice: multi-scale image data for calibrating remote-sensing-based winter wheat monitoring methods. Scientific Data 2024 11:1, 11(1), 1033-. https://doi.org/10.1038/s41597-024-03842-8

Badgley, G., Field, C. B., & Berry, J. A. (2017). Canopy near-infrared reflectance and terrestrial photosynthesis. Science Advances, 3(3). https://doi.org/10.1126/SCIADV.1602244/SUPPL_FILE/1602244_SM.PDF

Breunig, F. M., Galvão, L. S., Dalagnol, R., Dauve, C. E., Parraga, A., Santi, A. L., et al. (2020). Delineation of management zones in agricultural fields using cover–crop biomass estimates from PlanetScope data. International Journal of Applied Earth Observation and Geoinformation, 85, 102004. https://doi.org/10.1016/J.JAG.2019.102004

Canata, T. F., Wei, M. C. F., Maldaner, L. F., & Molin, J. P. (2021). Sugarcane Yield Mapping Using High-Resolution Imagery Data and Machine Learning Technique. Remote Sensing 2021, Vol. 13, Page 232, 13(2), 232. https://doi.org/10.3390/RS13020232

Colaço, A. F., Pagliuca, L. G., Romanelli, T. L., & Molin, J. P. (2020). Economic viability, energy and nutrient balances of site-specific fertilisation for citrus. Biosystems Engineering, 200, 138–156. https://doi.org/10.1016/J.BIOSYSTEMSENG.2020.09.007

Cunha, I. A., Baptista, G. M. M., Prudente, V. H. R., Melo, D. D., & Amaral, L. R. (2024). Integration of Optical and Synthetic Aperture Radar Data with Different Synthetic Aperture Radar Image Processing Techniques and Development Stages to Improve Soybean Yield Prediction. Agriculture 2024, Vol. 14, Page 2032, 14(11), 2032. https://doi.org/10.3390/AGRICULTURE14112032

Farid, H. U., Bakhsh, A., Ahmad, N., Ahmad, A., & Mahmood-Khan, Z. (2016). Delineating site-specific management zones for precision agriculture. The Journal of Agricultural Science, 154(2), 273–286. https://doi.org/10.1017/S0021859615000143

Filippi, P., Han, S. Y., & Bishop, T. F. A. (2024). On crop yield modelling, predicting, and forecasting and addressing the common issues in published studies. Precision Agriculture 2024 26:1, 26(1), 8-. https://doi.org/10.1007/S11119-024-10212-2

Fiorio, P. R., Silva, C. A. A. C., Rizzo, R., Demattê, J. A. M., Luciano, A. C. dos S., & Silva, M. A. da. (2024). Prediction of leaf nitrogen in sugarcane (Saccharum spp.) by Vis-NIR-SWIR spectroradiometry. Heliyon, 10(5), e26819. https://doi.org/10.1016/J.HELIYON.2024.E26819

Georgi, C., Spengler, D., Itzerott, S., & Kleinschmit, B. (2017). Automatic delineation algorithm for site-specific management zones based on satellite remote sensing data. Precision Agriculture 2017 19:4, 19(4), 684–707. https://doi.org/10.1007/S11119-017-9549-Y

Huete, A. R., Liu, H. Q., Batchily, K., & Van Leeuwen, W. (1997). A comparison of vegetation indices over a global set of TM images for EOS-MODIS. Remote Sensing of Environment, 59(3), 440–451. https://doi.org/10.1016/S0034-4257(96)00112-5

Kerry, R., Ingram, B., Oliver, M., & Frogbrook, Z. (2024). Soil sampling and sensed ancillary data requirements for soil mapping in precision agriculture I. delineation of management zones to determine zone averages of soil properties. Precision Agriculture 2024 25:3, 25(3), 1181–1211. https://doi.org/10.1007/S11119-023-10107-8

Khosla, R., Inman, D., Westfall, D. G., Reich, R. M., Frasier, M., Mzuku, M., et al. (2008). A synthesis of multi-disciplinary research in precision agriculture: site-specific management zones in the semi-arid western Great Plains of the USA. Precision Agriculture 2008 9:1, 9(1), 85–100. https://doi.org/10.1007/S11119-008-9057-1

Kross, A., Znoj, E., Callegari, D., Kaur, G., Sunohara, M., Lapen, D. R., & McNairn, H. (2020). Using Artificial Neural Networks and Remotely Sensed Data to Evaluate the Relative Importance of Variables for Prediction of Within-Field Corn and Soybean Yields. Remote Sensing 2020, Vol. 12, Page 2230, 12(14), 2230. https://doi.org/10.3390/RS12142230

Li, Y., Miao, Y., Rawat, A., Stueve, K., & Cao, W. (2025). Identifying key soil and landscape factors influencing yield spatial patterns for management zone delineation using ensemble machine learning. Computers and Electronics in Agriculture, 237, 110487. https://doi.org/10.1016/J.COMPAG.2025.110487

Lin, S., Li, J., Liu, Q., Li, L., Zhao, J., & Yu, W. (2019). Evaluating the Effectiveness of Using Vegetation Indices Based on Red-Edge Reflectance from Sentinel-2 to Estimate Gross Primary Productivity. Remote Sensing 2019, Vol. 11, Page 1303, 11(11), 1303. https://doi.org/10.3390/RS11111303

Maimaitijiang, M., Sagan, V., Sidike, P., Maimaitiyiming, M., Hartling, S., Peterson, K. T., et al. (2019). Vegetation Index Weighted Canopy Volume Model (CVMVI) for soybean biomass estimation from Unmanned Aerial System-based RGB imagery. ISPRS Journal of Photogrammetry and Remote Sensing, 151, 27–41. https://doi.org/10.1016/J.ISPRSJPRS.2019.03.003

Maldaner, L. F., Molin, J. P., & Spekken, M. (2021). Methodology to filter out outliers in high spatial density data to improve maps reliability. Scientia Agricola, 79(1), e20200178. https://doi.org/10.1590/1678-992X-2020-0178

Massruhá, S. M. F., Leite, M. A. A., Oliveira, S. R. M., Meira, C. A., Luchiari Junior, A., & Bolfe, É. L. (2020). Agricultura digital: pesquisa, desenvolvimento e inovação nas cadeias produtivas. Portal Embrapa. www.embrapa.br/fale-conosco/sac

McNaull, R. P., & Darr, M. J. (2020). Large-Scale Field Study of Impact-Based Yield Monitor Performance. Applied Engineering in Agriculture, 36(2), 197–204. https://doi.org/10.13031/AEA.13527

Miao, Y., Mulla, D. J., & Robert, P. C. (2018). An integrated approach to site-specific management zone delineation. Frontiers of Agricultural Science and Engineering, 5(4), 432–441. https://doi.org/10.15302/J-FASE-2018230

Mohammed, G. H., Colombo, R., Middleton, E. M., Rascher, U., van der Tol, C., Nedbal, L., et al. (2019). Remote sensing of solar-induced chlorophyll fluorescence (SIF) in vegetation: 50 years of progress. Remote Sensing of Environment, 231, 111177. https://doi.org/10.1016/J.RSE.2019.04.030

Moharana, P. C., Jena, R. K., Pradhan, U. K., Nogiya, M., Tailor, B. L., Singh, R. S., & Singh, S. K. (2020). Geostatistical and fuzzy clustering approach for delineation of site-specific management zones and yield-limiting factors in irrigated hot arid environment of India. Precision Agriculture, 21(2), 426–448. https://doi.org/10.1007/S11119-019-09671-9/TABLES/6

Molin, J. P., Amaral, L. R., & Colaço, A. F. (2015). Agricultura De Precisão. Oficina de Textos.

Mulla, D. J. (2013). Twenty five years of remote sensing in precision agriculture: Key advances and remaining knowledge gaps. Biosystems Engineering, 114(4), 358–371. https://doi.org/10.1016/J.BIOSYSTEMSENG.2012.08.009

Nawar, S., Corstanje, R., Halcro, G., Mulla, D., & Mouazen, A. M. (2017). Delineation of Soil Management Zones for Variable-Rate Fertilization: A Review. Advances in Agronomy, 143, 175–245. https://doi.org/10.1016/bs.agron.2017.01.003

Ouazaa, S., Jaramillo-Barrios, C. I., Chaali, N., Amaya, Y. M. Q., Carvajal, J. E. C., & Ramos, O. M. (2022). Towards site specific management zones delineation in rotational cropping system: Application of multivariate spatial clustering model based on soil properties. Geoderma Regional, 30, e00564. https://doi.org/10.1016/J.GEODRS.2022.E00564

Pathak, H. S., Brown, P., & Best, T. (2019). A systematic literature review of the factors affecting the precision agriculture adoption process. Precision Agriculture, 20(6), 1292–1316. https://doi.org/10.1007/s11119-019-09653-x

Rokhafrouz, M., Latifi, H., Abkar, A. A., Wojciechowski, T., Czechlowski, M., Naieni, A. S., et al. (2021). Simplified and hybrid remote sensing-based delineation of management zones for nitrogen variable rate application in wheat. Agriculture (Switzerland), 11(11), 1104. https://doi.org/10.3390/AGRICULTURE11111104/S1

Shilpa, S., Shailaja, K. P., Nischitha, S. G., Hegde, N. V., & Teja, K. K. (2025). External Clustering Validation using ARI, NMI and FMI. ITM Web of Conferences, 79, 01004. https://doi.org/10.1051/ITMCONF/20257901004

Silva, E. R. O. da, Silva, T. L. da, Wei, M. C. F., Souza, R. A. de, & Molin, J. P. (2025). Spatial and Temporal Variability Management for All Farmers: A Cell-Size Approach to Enhance Coffee Yields and Optimize Inputs. Plants, 14(2), 169. https://doi.org/10.3390/PLANTS14020169/S1

Sterle, L. G. G., & Molin, J. P. (2025). Management Zones for Irrigated and Rainfed Grain Crops Based on Data Layer Integration. Agronomy 2025, Vol. 15, Page 1864, 15(8), 1864. https://doi.org/10.3390/AGRONOMY15081864

Verrelst, J., Malenovský, Z., Van der Tol, C., Camps-Valls, G., Gastellu-Etchegorry, J. P., Lewis, P., et al. (2019). Quantifying Vegetation Biophysical Variables from Imaging Spectroscopy Data: A Review on Retrieval Methods. Surveys in Geophysics, 40(3), 589–629. https://doi.org/10.1007/S10712-018-9478-Y

Weiss, M., Jacob, F., & Duveiller, G. (2020). Remote sensing for agricultural applications: A meta-review. Remote Sensing of Environment, 236, 111402. https://doi.org/10.1016/J.RSE.2019.111402

Yu, Z., Chen, Q., Shan, Q., Lv, Y., Chen, Z., Zhou, Y., et al. (2025). Developing soybean yield prediction model based on multicolor space and texture features of UAV images. Computers and Electronics in Agriculture, 235, 110345. https://doi.org/10.1016/J.COMPAG.2025.110345